# Effects of the Geometric Constraints on the Size Distributions of Debris in Asteroidal Fragmentation

Adriano Campo Bagatin and Jean-Marc Petit

Centre National de la Recherche Scientifique,

Observatoire de la Côte d'Azur, B.P. 4229, 06304 Nice Cedex 4, France

petit@obs-nice.fr

Submitted to *Icarus*
Revised version: 16 August 2000

**length:**
- 22 manuscript pages
- 2 tables
- 7 figures on 8 pages

**Proposed running title**: Geometric Constraints in Asteroidal Fragmentation

Send proofs to:

Jean-Marc Petit
Observatoire de Nice
B.P. 4229
F-06304 Nice Cedex 4 France

Tel: +33 4 92 00 30 89
Fax: +33 4 92 00 30 33
Internet: petit@obs-nice.fr

**Abstract**

It is commonly accepted that the formation of asteroid families is the consequence of catastrophic impacts on former *parent bodies* (Hirayama, 1933). But to reproduce the puzzling steep size distributions of the presently known asteroid families has been up to now a task in which recent modelling techniques of fragmentation have typically failed. The role of geometric constraints in the production of fragments in asteroidal collisions is an issue that has been investigated in recent times only by Tanga *et al.* , 1999, and that might give some insight into the understanding of high–velocity collisional processes.

Improvements to the approach by Tanga *et al.* are introduced in the present work, in order to take into account in a more realistic way the different shapes that largest remnants may have when formed in high–velocity collisional events involving spherical parent bodies. We also consider the case in which the parent body and the largest remnant are cubes and the fragments are *a)* cubes, *b)* parallelepipeds, instead of spheres.

A somewhat uniform power–law behaviour in the size distributions of the randomly–generated fragments is found in the numerical simulations—not detected by Tanga *et al.* —and an analytical derivation of the upper limit to the corresponding exponent is given.

Further improvements are introduced in the model in order to refine it and to allow any fragment to develop any shape, and to account for the fact that fragments form more or less at the same time, not sequentially.

Finally, the results of the refined model are compared with the size distributions of the observed actual main belt asteroid families, and encouraging agreement is obtained in most cases.



**Keywords**: Asteroids - Collisions - Origin, solar system - Planetesimals

# I Introduction

It has been recently pointed out that the size distributions of asteroid families in the Asteroid Belt is much steeper (Zappalá and Cellino, 1996) than the one expected for a collisionally relaxed population (Dohnanyi, 1969). The need for finally finding a reliable model for the fragmentation of asteroidal bodies, able to explain the steep size distributions of fragments coming from family–forming impacts, is a current issue for many reasons. First of all it is important in understanding the collisional processes going on among small solar system objects. In fact, many numerical models on the collisional evolution of asteroids are fed by fragmentation models that, even if self–consistent and theoretically correct (e.g: Petit and Farinella, 1993), typically fail to reproduce family distributions. On the other hand, having a good agreement between fragmentation model predictions and actual family distributions is needed to study in detail and in a quantitative way how many fragments are ejected into resonant orbits and into dynamically instable regions, in order to know more about the Near Earth Asteroid population.

The "geometric approach" to this problem, explained by Tanga *et al.* , is a very interesting *heuristic* one. The idea that geometric constraints may play a role in the production of fragments can be loosely found in the literature since the 30's by Rosin and Rammler (1933), Lienau (1936), Mott (1947), Gilvarry (1961), and Gradie (1978), in whose works the principles of geometric statistical fragmentation underlie. In the past decade Grady & Kipp (1985) recovered the idea, and report many sets of numerical experiments that were performed in order to obtain the distributions of debris in the fragmentation of square surfaces. In those works, however, it had not been pointed out that the geometric boundaries of surfaces and volumes may affect the final statistical distribution of the produced fragments.

As it will be a reference in the paper, we will now give a short outline of Tanga *et al.* model. They start from a spherical parent body and choose a value for the ratio ($f_{LR}$) of the volume of the largest remnant to the volume of the parent body; accordingly they draw another sphere –internally tangent to the parent body– representing the largest remnant. Then, they draw at random one point within the available volume inside the parent body, but outside the largest remnant, and they produce a sphere whose radius is as large as possible with the constraints of being inside the parent body and not overlapping with another fragment. Other random points are then sequentially drawn and the corresponding fragments are always grown in the same way. Every "new" growing sphere has then the constraints due to the presence of the formerly created spherical fragments. The process ends when they reach a given number of fragments.

The way the volume of the largest fragment is taken into account is, as it turns out, a critical point in the model proposed by Tanga *et al.* To consider it to be of spherical shape internally tangent to the parent body volume is an unrealistic assumption in general, especially in the case of cratering. In fact, for high ratios of the mentioned volumes, the remaining volume available for the random creation of fragments is only a thin shell around the largest remnant itself. Now, this would be more or less realistic only in the case in which the result of the impact would be the "spallation" of material, that is the ejection of shell–like fragments from all around the surface of the target. These events are described in laboratory experiments, and probably happen in asteroidal collisions, but they seem to be characteristic of low–velocity impact events, rather than high–velocity collisions. A characteristic feature of this model, and an expected result of it, is the production of a large number of fragments of about the same size, resulting in a steep cumulative size distribution of fragments at the largest sizes. The consequences of this way of modelling the process are: *i)* the randomly generated second largest fragment is very small with respect to the largest remnant; so, reproducing the asteroid families' distributions often requires fixing the size of the second largest fragment as well, and this means constraining the model in an artificial way; *ii)* the greater $f_{LR}$ is, the steeper the distribution of the largest fragments is; *iii)* the reconstructed volume is relatively small in many cases, due to the difficulty of finding available space for relatively large fragments to be created.

In the general case, the results of a high–velocity collision among solar system objects range from the formation of a crater on the surface of the target, to a catastrophic fragmentation, depending on the energy of the impacting body, and on the characteristics of the target itself.

Thus we improved Tanga *et al.* model in three main ways.

a) We simulated the shape of the largest remnant in a way (described in sec. II) to have different shapes and a continuous transition –depending on the desired mass ratio– from a small crater to a large bowl to a convex largest fragment shape, ending up with a spherical largest remnant. After running the numerical simulations we happen to obtain a well–defined power–law for the size distribution of fragments. The comparison between the present model results and Tanga *et al.* 's are shown in sec. III. In order to underline that the above objections to Tanga *et al.* model are somewhat general, we used their approach with cubic targets and fragments, and with parallelepipedic fragments, and we obtained the same pattern as they did (sec. IV). An analytical explanation of the well–defined power–law behaviour can be found in sec. V.

b) Two further improvements were introduced into the model. First of all, we allow for as many possible shapes for the largest remnant as suggested by many experiments. The shape of the largest remnant can vary according to material properties and impact modalities: these shapes can be roughly approximated as an antipodal or a core sphere, or instead an intersection of spheres, but it can also have a cone–like shape, as seen in some experiments. Moreover, in an effort of better mimicking true fragmentation processes, we modified our model in a way to be able of producing many fragments at the same time, instead of one-at-a-time.

c) We allow for fragments of any shape. In fact, the way we perform the growth of any set of fragments do not constrain their shape in a defined way.

The explanation of this model will be given in sec. VI.

As a main result of our model we have that many of the best reliable asteroid family distributions can be matched fairly well as far as the largest ten or so fragments are concerned.

The conclusions about the results obtained in this work are finally discussed in sec. VII.

# II The Shape of the Largest Remnant

As mentioned in the Introduction, we consider that instead of having spheres for the shape of largest remnants resulting from high–velocity collisions for any value of $f_{LR}$, it is more realistic to have the possibility of changing those shapes as $f_{LR}$ varies. We can then simulate such shapes to be spheres (for small $f_{LR}$) or crater shapes (for large $f_{LR}$). In order to get a continuous transition in the shape of a largest remnant, the idea is to model its surface as the union of parts of the surface of two different spheres. Obviously, one of the spheres is the parent body. The other one is a sphere which radius and centre are specified as explained below. The intersection of the surfaces of the two spheres determines the shape of the largest remnant.

Let us consider the parent body as a sphere of unit radius centred at the origin of an abscissa axis. This sphere then cuts the axis at -1 and 1. The second sphere is also centred on the same axis; let us call $x_c$ the coordinate of its centre, and $R_c$ its radius. The way $x_c$ and $R_c$ are chosen is purely arbitrary and driven solely by the desire that the excavation be bowl–shaped for large $f_{LR}$ and convexe-shaped for smaller $f_{LR}$, changing continuously with $f_{LR}$ and ending up as an internally tangent sphere for the very small $f_{LR}$'s. The limit for large $f_{LR}$ is chosen so that a crater is at most 10 to 15% of the volume of the parent body. The limit for an internally tangent sphere is more arbitrary, and we choose the value $f_{LR} = 1/8$. We therefore consider three different cases:

1) Concave excavation in the parent body. We take $x_c > 1$ and

$$R_c = x_c - \frac{1}{2} - \frac{1}{2x_c} \tag{1}$$

In this way the deepest point of the excavation reaches the abscissa $1/2+1/(2x_c)$, always in the interval $[1/2, 1]$. When $x_c \to \infty$, the sphere becomes a plane and the largest remnant has a flat side at $x = 1/2$.

Let's call $x_0$ the $x$ coordinate of the intersection plane of the two spheres. It is straightforward to obtain that

$$x_0 = (1 - R_c^2 + x_c^2)/(2x_c), \tag{2}$$

so we have:

$$x_0 = \frac{4x_c^3 + 7x_c^2 - 2x_c - 1}{8x_c^3} \tag{3}$$

Correspondingly, the volume of the largest remnant so defined is:

$$V = \frac{\pi(40x_c^5 - 99x_c^4 + 60x_c^3 + 14x_c^2 - 12x_c - 3)}{192x_c^5} \tag{4}$$

The minimum volume of the concave largest remnant (that coincides with the maximum volume of the convex largest remnant) is therefore $V = \frac{9\pi}{8}$, and the corresponding mass fraction with respect to the parent body is $f_{LR} = \frac{27}{32}$.

2) Convex largest remnant, intersection of two spheres. Here we take $x_c \leq -\frac{1}{2}$, and

$$R_c = -x_c + \frac{1}{2} + \frac{1}{4x_c} \tag{5}$$

From Eq. 2, we find that

$$x_0 = \frac{16x_c^3 + 20x_c^2 - 4x_c - 1}{32x_c^3} \tag{6}$$

Here again, as $x_c \to -\infty$, the largest remnant has a flat side, corresponding to the limit of the previous case. At the other limit, when $x_c = -1/2$, $x_0 = -1$ and $R_c = 1/2$, corresponding to a completely spherical largest remnant.

Correspondingly, the volume of the largest remnant so determined is:

$$V = \frac{\pi(3456x_c^5 + 1008x_c^4 - 384x_c^3 - 40x_c^2 + 24x_c + 3)}{3072x_c^5} \tag{7}$$

The minimum volume of the non–spherical convex largest remnant is then $V = \frac{\pi}{6}$, that corresponds to a fraction of mass respect to the parent body $f_{LR} = \frac{1}{8}$. This case represents a more general shattering event.

3) Spherical largest remnant. For $f_{LR} < 1/8$, the largest remnant is simply a sphere, internally tangent at $x = -1$ to the parent body. Therefore, $x_c \in [-1, -1/2]$, and $R_c = x_c + 1$.

Figure 1 shows a section of the spheres by a plane containing the $x$-axis. The solid line contours the largest remnant while the dashed lines represent the rest of the spheres. Figure 1a corresponds to the first case, with $f_{LR} \geq 27/32$, Fig. 1b to the second case, with $27/32 \geq f_{LR} \geq 1/8$ and Fig. 1c to the third case, with $1/8 \geq f_{LR}$. As can be seen here, we no longer have the problem of the volume available for secondary fragments being a thin shell. These shapes fall within the wide range of impact experiment data. In addition, the exact shapes and limits have little effect on the outcome of the simulations. The only important point here is to avoid the thin shell effect for large $f_{LR}$'s. Such a thin shell would correspond to a spallation, but to our knowledge, spallation do not occur for $f_{LR}$ larger than 90%.

# III Comparison Between the Results

In this section we compare the results of the present model to those obtained by Tanga *et al.* (1999). In the present model, the secondary fragments are chosen in the same way as in Tanga *et al.* . The only difference lies in the shape of the largest remnant. For each value of $f_{LR}$ in 0.1, 0.3, 0.5, 0.7, 0.9, we have run 20 simulations with our model, generating 30000 fragments in each run, but changing the random number generator seed. These sets of 20 runs allow to extract the statistically significant characteristics of the distributions.

In order to test the dependence of these on the number of generated fragments, we have performed simulations with 200000 or more fragments for each value of $f_{LR}$, with no noticeable change in the distribution, except for the extension of the distribution to smaller size fragments. Figure 2 shows the size distribution of fragments for one simulation for each value of $f_{LR}$.

The main differences found between our results and those of Tanga *et al.* (1999) are:

1) In the present model the ratio of the size of the second largest fragment to the size of the parent body (Fig. 3, open circles) for any value of $f_{LR}$ is larger than that obtained in Tanga *et al.* model (Fig. 3, solid circles).

This difference is a direct consequence of our model avoiding the thin shell effect. The size of the second largest fragment is limited by the thickness of the available volume, which can be very small in the Tanga *et al.* model. Even though more physical, this assumption does not seem to give better fits to the observed asteroid families (see sec. VI.B)

2) For the same number of fragments, we recover a larger fraction of the total mass of the parent body (Fig. 4, open circles: this model; solid circles: Tanga *et al.* model). This again is a consequence of the thicker available volume for secondary fragments, allowing for larger fragments.

3) An interesting overall pattern arising in the simulations is that the cumulative size distributions of fragments, for each value of $f_{LR}$, tend to follow approximately a power–law with the same value of the exponent of $\sim$-2.73 (Fig. 5), in a range between the largest 300 and 3000 fragments. For smaller fragments, a flattening in the distribution appears. This contrasts with Tanga *et al.* work, that shows a different behaviour in the cumulative size distribution of fragments, as a function of $f_{LR}$, at larger sizes. In their model, however, if the number of generated fragments is increased, a "power–law range" is also obtained, between a flattening of the distribution at small sizes and the steep size distribution due to the thin–shell effect at greater sizes.

An analytical derivation of this well defined power–law in the size distribution of the produced fragments is given in sec. V. The power–law pattern is followed –in the small size range– by a flattening in the size distribution. This flattening occurs due to the finite number of fragments generated in the simulation and is also reproduced in the analytical derivation of sec. V.

# IV From Spheres to Cubes and Parallelepipeds

In order to investigate the dependence of the model on the shape of the parent body and the fragments, we have modified it and performed sets of numerical experiments substituting spheres with *a)* cubic parent bodies and fragments, and *b)* cubic or parallelepipedic parent bodies and parallelepipedic fragments. The secondary fragments are chosen in the same way as before. In the case of parallelepipeds, the ratio between the length of their axes is chosen at random, such that $A_{\max}/A_{\min} \leq 3$, where $A_{\max}$ and $A_{\min}$ are the maximum and minimum length. All the cubes and parallelepipeds (parent body, largest remnant, secondary fragments) have their sides parallel to the $x$, $y$ and $z$ axes. The largest remnant has a cubic shape in all these simulations. The shapes of fragments coming from catastrophic fragmentation of experimental targets have been shown to be roughly tri–axial objects, with a loose relationship between the three axes of the kind $1 : \sqrt{2} : 2$, this trend has been confirmed also by Paolicchi *et al.* , 1996. In the present simulations, we have left fragments free to have any parallelepipedic shape within the range of axes ratios from 1 to 3, to minimize the number of deterministic constraints into the model, and to avoid at the same time very unlikely “stick–like” or “tile–like” shapes for fragments.

In these two sets of simulations we obtained cumulative distributions with overall patterns very similar (almost indistinguishable) to the ones obtained by Tanga *et al.* , that is a large ratio between the second largest fragment and the largest remnant, and distributions depending on $f_{LR}$ in the largest fragments range. In fact in the present cases the largest remnants are cubes, so the space left for the production of other fragments is again a shell, which is rather thin when $f_{LR}$ is large.

On the other hand, in the ’cubes’ case the recovering of volume is better than in the ’spheres’ case, and in the ’parallelepipeds’ case the recovered volume is much higher than in all other cases, as shown in Table 1.

The effect of the largest remnant in limiting the thickness of the available volume for the secondary fragments, and therefore their size, seems then to be a general one and it seems to be responsible for this kind of pattern, independently on the shape of the parent body and fragments.

However, one can note that when a number of fragments large enough is created, again a single power–law is detected at intermediate fragment sizes, followed by a flattening in the size distribution, according to the analythical model described in sec. V.

# V Analythical Derivation of the Power–law Behaviour

In this section we derive analytically the shape of the size distribution function of the fragments.

## V.A Definitions

Let us call $f(n,r)dr$ the number of spheres with radius between $r$ and $r+dr$, when $n$ spheres have already been generated. We have

$$\int_0^{r_{\max}} f(n,r)\, dr = n, \tag{8}$$

where $r_{\max}$ is the maximum value of $r$. This is not a critical value, as it disappears in the end results. One could, for example, estimate it from the initial available volume.

The probability that sphere $n$ has a radius between $r$ and $r + dr$ is

$$p(n,r)dr = f(n,r)dr - f(n-1,r)\,dr \simeq \frac{\partial f}{\partial n}\,dr. \tag{9}$$

The total volume occupied by spheres is

$$u(n) = \int_0^{r_{\max}} C_v r^d f(n,r)\,dr, \tag{10}$$

where $d$ is the dimensionality of the space (generally either 3 or 2) and $C_v$ the coefficient giving the "volume" of a "sphere" in a $d$- dimensional space. When $d = 3$, $C_v = 4\pi/3$, while for $d = 2$, $C_v = \pi$.

For $n \to \infty$, $f(n,r)$ tends to an asymptotic distribution $f(\infty, r)$. We make here the natural assumption that when $n \to \infty$, then $u(n) \to V$, the initial volume of the available space for secondary fragments. In other words,

$$u(\infty) = \int_0^{r_{\max}} C_v r^d f(\infty,r)\,dr = V. \tag{11}$$

The available volume to put new spheres in is then

$$v(n) = V - u(n) = \int_0^{r_{\max}} C_v r^d \left[f(\infty,r) - f(n,r)\right]\,dr. \tag{12}$$

The total surface of the current spheres is

$$s(n) = \int_0^{r_{\max}} C_s r^{d-1} f(n,r)\,dr, \tag{13}$$

where $C_s = 4\pi$ when $d = 3$, and $C_s = 2\pi$ when $d = 2$. Note that we have the relation $C_v = C_s/d$. Let us call $S$ the surface of the boundary of volume $V$. Considering a very small $r$, the volume occupied by points within the available volume and at a distance smaller than $r$ from either a sphere or from the boundary $S$ is simply $[s(n) + S]\,r$. Hence, for very small $r$,

$$p(n,r)dr = \frac{[s(n) + S]\;dr}{v(n)}. \tag{14}$$

## V.B Approximation of $f$

Given the results of the simulation, we suppose that the asymptotic distribution is a power law:

$$f(\infty, r) = a r^{-\nu-1}, \tag{15}$$

where $a$ and $\nu$ are constantes. $\nu$ must be smaller than $d$, otherwise the total volume of spheres would diverge for $r \to 0$.

Note that approximation Eq. 15 is well satisfied for small $r$, but not when $r$ is close to $r_{\max}$. This is of no real importance, since in the expression Eq. 12 of $v(n)$, the term in brackets vanishes for large $r$ (it is no longer possible to create large spheres); and in expression Eq. 13 of $s(n)$, the small values of $r$ are dominant as long as $\nu > d-1$.

We use an extra approximation for $f(n,r)$. For large $r$, $f(n,r)$ is very close to $f(\infty,r)$, so we use Eq. 15. For small $r$, $f(n,r)$ is smaller than $f(\infty,r)$: the filling up with small spheres is not yet complete. Equation 14 shows that $\frac{\partial f}{\partial n}$ is independent on $r$ for small $r$; hence $f(n,r)$ is also constant for small $r$. This suggests the following approximation:

$$f(n,r) = \begin{cases} ar^{-\nu-1} & \text{for } r > \rho(n), \\ a\rho^{-\nu-1} & \text{for } r < \rho(n), \end{cases} \tag{16}$$

where $\rho(n)$ is a decreasing function of $n$. It follows that

$$p(n,r) = \frac{\partial f}{\partial n} = \begin{cases} 0 & \text{for } r > \rho(n), \\ -a(\nu+1)\rho^{-\nu-2}\dfrac{d\rho}{dn} & \text{for } r < \rho(n). \end{cases} \tag{17}$$

We have:

$$1 = \int_0^{r_{\max}} p(n,r)\,dr = -a(\nu+1)\rho^{-\nu-1}\frac{d\rho}{dn}. \tag{18}$$

Therefore, Eq. 17 reads

$$p(n,r) = \frac{\partial f}{\partial n} = \begin{cases} 0 & \text{for } r > \rho(n), \\ \rho^{-1} & \text{for } r < \rho(n). \end{cases} \tag{19}$$

## V.C The exponent $\nu$

It is now easy to compute $v(n)$ and $s(n)$, substituting Eq. 15 and Eq. 16 in Eq. 12 and Eq. 13. We get:

$$v(n) = \frac{C_s a(1+\nu)}{d(d+1)(d-\nu)}\rho^{d-\nu}, \tag{20}$$

$$s(n) = \frac{C_s a(1+\nu)}{d(\nu-d+1)}\rho^{d-1-\nu}. \tag{21}$$

Assuming that $\rho \to 0$ as $n \to \infty$, hence, we also have $s(n) \to \infty$, as long as $\nu > d-1$. We can therefore neglect $S$ in Eq. 14, and obtain, for small $r$:

$$p(n,r)\,dr = \frac{(d+1)(d-\nu)}{(\nu-d+1)}\rho^{-1}\,dr. \tag{22}$$

Comparing with Eq. 19, we get:

$$\frac{(d+1)(d-\nu)}{(\nu-d+1)} = 1, \tag{23}$$

which yields:

$$\nu = \frac{d^2+2d-1}{d+2}. \tag{24}$$

In the 3 dimensional case, $d = 3$ and $\nu = 14/5 = 2.8$ which is close to the experimentally obtained value.

Actually, the exponents of the power–law obtained by our simulations are slightly smaller than the one obtained here (Fig. 5). This discrepancy was to be expected. In Eq. 14 the volume available for spheres of radius $r$ is smaller than $[s(n) + S]r$ since the already created spheres are in contact and hence not all the surface $s(n) + S$ is available for spheres of radius $r$. Thus the right hand term in Eq. 23 is $\alpha > 1$. It turns out that the solution for $\nu$ given in Eq. 24 is a decreasing of $\alpha$, therefore leading to a value of $\nu$ smaller than 14/5.

In the case of cubes or parallelepipeds of fixed aspect ratio, the derivation would be identical, with only a change in the values of $C_v$ and $C_s$, which do not change the value of $\nu$.

## V.D Functions of $n$

As a byproduct, we can explicitly derive $\rho(n)$, $v(n)$ and $s(n)$, which we do for $d = 3$ The differential equation Eq. 18 can be integrated to:

$$\rho = \left[\frac{\nu n}{a(\nu+1)}\right]^{-1/\nu} = \left(\frac{14n}{19a}\right)^{-5/14}. \tag{25}$$

Substituting in (20) and (21), we obtain:

$$v(n) = \frac{19a\pi}{3}\left(\frac{14n}{19a}\right)^{-1/14}, \tag{26}$$

and

$$s(n) = \frac{19a\pi}{3}\left(\frac{14n}{19a}\right)^{2/7}. \tag{27}$$

Note that the available volume $v(n)$ decreases very slowly as $n$ increases. This is confirmed by the simulations.

# VI The "3–D Grid" Model

From the previous results, two main conclusions can be drawn. First of all, only the few hundred largest fragments generated by this kind of algorithm really depend on the input parameters. For smaller size fragments, the size distribution is a power–law whose parameters are determined by the algorithm itself. So there is no point in allowing for very small and numerous fragments. The second point is that the actual shape of the largest remnant is of importance. Hence the purely analitycal determination of fragments as spheres is not a practical way of simulating the fragmentation process. We rather need to introduce a new model, based on a "finite-difference" kind of approach.

## VI.A The model

We therefore consider a cubic discretization of space and introduce the following new characteristics in the model.
a) In addition to its size (given by $f_{LR}$), the largest fragment is also defined by its shape (antipodal or core sphere, intersection of spheres, straight edge cone–like shape, concave cone–like shape), and location.
b) Fragments do not develop sequentially, i.e. one at a time, but rather they grow $n$ at a time, where $n$ is any given integer input parameter.
c) Fragments can have any shape, in principle, due to the way they are created.

The practical implementation of the model is as follows:

1. We consider a 3D cubic grid of typically 200×200×200 cells. We tested the effect of resolution with grids from 100×100×100 to 400×400×400 and found no meaningfull changes in the outome of the model.

2. A triaxial ellipsoid parent body centred in the middle of the cubic grid is selected. All the cells falling inside the parent body are marked available for fragments. In all the simulations presented here, we always used a spherical parent body.

3. The size, shape, and location of the largest fragment are given as input parameters and the cells belonging to it are marked accordingly.

   Now the remaining available space is ready to be filled with other fragments. Every fragment is labelled uniquely, in order to be able to distinguish it from the others.

4. A set of $n$ cells (typically 10 to 100) is drawn at random in the available space, as "seeds" for developing fragments, setting the ones that will be growing up at the same time.

5. For every such *proto*–fragment, checking of every closest neighbour is made: if a neighbour cell is available, that is if it doesn't belong to any other numbered fragment, nor it is outside the parent body, then it is labelled with the corresponding fragment number and of course is considered as belonging to it.

6. The model then skips to another "seed", the checkings of step 5 are made, and so on. Once all the neighbours of any given cell–fragment have been checked, up to the $n$–th fragment, we start again a new check round, going back to the first one in the set. In this way, as checkings are made only for the closest neighbour cells to any given fragment, we have a set of fragments growing *at the same time*, as we expect for real fragmentation, and not sequentially.

7. The growing of any single fragment is stopped either when there is no more "free" neighbouring cell, or when a certain number of neighbour cells are

found to belong to other fragments, or to be outside the parent body. This allows one fragment to have contact surfaces with one or more fragments. The limiting number of occupied neighbour cells is a function of the current size of the fragment, to avoid growing flat fragments.

8. Once one set of $n$ fragments is done, another $n$–cell set is drawn at random, and the growth process is started again.

   At last, when the total number of requested fragments is reached, or when their size is typically at the limit of resolution (say, one single cell), the fragment production ends.

Finally, all the fragments are given a size equivalent to a spherical fragment of the same volume. The size distribution of the fragments thus generated is finally compared to that of the observed families of asteroids. We scale the sizes so that the size of the largest fragment of the model corresponds to that of the largest member of the family.

Figure 6 presents a section of the grid, with some of the fragments created as explained above. We actually plot one out of four fragments. The rather square shape of the largest fragments (except for the very largest) is due to the closest neighbour growing scheme, which tends to create fragments with a regular octahedron shape. However, the actual final shape will adapt to the circumstances and follow the limits of the target (fragment at the top) or of another fragment (fragment along the largest one).

## VI.B Results

Many sets of simulations with the "3–D Grid" model have been performed, and a few general characteristics have been noticed.
i) No dependence of the results on the resolution of the 3–D grid supporting the model is found, within a reasonable range of cells ($10^6$ to $64\times10^6$).
ii) The model shows little sensitivity to the number $n$ of fragments that are generated at the same time: running from 10 to 100 doesn't seem to imply significant variations in the resulting cumulative distribution.
iii) The model seems instead to depend markedly on the shape of the largest remnant chosen in any given simulation. In general, core and antipodal spheres give a smaller second largest fragment and a steeper distributions for the largest fragments, with respect to other shape choices. This pattern is more obvious for large $f_{LR}$, in the case of spherical largest remnant shapes, due to the thin–shell effect already mentioned in sec. II.
iv) Three main patterns seem to show up as a general trend in the outcomes of the present way of handling with the simulation of fragmentation. First of all, it can be seen that we obtain a somewhat random distribution for about the ten to one hundred largest fragments; this range is followed by a "straight" distribution for smaller fragments, apparently following a power law of the kind shown in sec. V, with an exponent that may slightly vary around the value -2.9, depending on the

shape of the largest remnant and on $f_{LR}$; finally a characteristic flattening of the distribution is found for the smallest size range. It is obvious that the largest fragments behaviour is due to the stochastic nature of the location of the seed cells at the beginning of the fragment growth process in the model. The intermediate size range behaviour, i.e. a power–law size distribution, is a reminiscence of the effect described in sec. V. As for the behaviour of the smallest size fragments, it is due to the finite number of fragments we allow for in the simulations, and to the growth–stop criterion we adopt. In fact, when the available space for new fragments is small, the fragments produced have smaller and smaller number of cells, as their growth is stopped earlier and earlier by finding that many neighbour cells are already occupyed by other fragments.

The main characteristics of the size distribution of about half among 18 reliable asteroid families seem to be reproduced by the present model, especially at the largest size range, corresponding roughly to the size range above the so–called "completeness diameter" of the families. The completeness diameter of a given family is an estimate of the size above which we expect to know all the members of that family. This value is "guessed" from what we believe is the absolute magnitude completeness limit at a given heliocentric distance, and estimates of the albedo of asteroids as a function of taxonomic types and diameters. The slope of the overall average size distribution of fragments is also in good agreement with the available data for asteroid families. The best results of the present model are obtained for cases in which the largest remnant to parent body mass ratio ($\mathrm{f}_{LR}$) is supposed to be small ($\leq 0.3$).

The formation of the largest fragments in laboratory impact experiments does not seem to follow a well–defined pattern of size distribution; it rather seems to be governed by the stochastic coalescence of flaw propagation within the target as the shock wave induced by the impact propagates through the target itself. This means that given many targets of the same fixed size, impacted by the same kind of projectile at the same impact speed, the distribution of every single set of the largest fragments have slightly different, undefined size distributions, due to the nature of the fragmentation process itself. Now, if we are to simulate an analogous process numerically, and we intend to fit the size distribution of the largest fragments of a given family, we have to follow a *trial and error* technique, that is we have to try and find which one, among a set of simulations of the same kind, results to be closer to a given family size distribution. In the case of the fits presented here, we have just run a few simulations in every case, changing $\mathrm{f}_{LR}$ and/or the shape of the largest remnant. Re–running a simulation with a fixed set of parameters only changes the details of the largest fragments distribution, but does not substantially change the overall look of the results. Anyway it has to be said that the presented set of data fits by the model is just one – not necessarily the best – among the possible ones.

Let us now comment the results of the fits to some of the asteroid families, among which we include some of the best known ones (Eos, Themis, Koronis and Maria).

For each family a few observational data and characteristics are given, such as the size of the largest observed member ($D_{LR}$), the completeness diameter ($d_C$), the ratio between the two largest members ($D_2/D_{LR}$), and eventually the most remarkable patterns of its size distribution. The results of the model are summarized in terms of the 'Largest Fragment Mass/Parent Body Mass' ($f_{LR}$), and in terms of parent body size ($D_{PB}$) and shape of the largest remnant. A summary of these data is given in Table 2.

In the case of family data, the bending in size distributions is an effect of incompleteness due to observational biases.

- *EOS* (Fig. 7a) – *Observations*: $D_{LR} = 103.9$ km. $d_C \approx 17$ km. $D_2/D_{LR} = 0.84$. No objects between 50 and 70 km.

*Model*: $f_{LR} = 0.1$. $D_{PB} \approx 240$ km. Largest remnant shape: Antipodal Sphere.

The model reproduces rather well the overall size distribution, including some details of the structure of it, such as the lack of objects around 60 km.

Were the model a realistic estimate of how fragments size do distribute after catastrophic fragmentation, it would imply that little collisional evolution had occurred since then.

This might then be a very young family, and the event that originated it would have occurred a few hundred Myr ago. A similar loose age estimate has been previously suggested by Farinella *et al.* , 1996.

- *KORONIS* (Fig. 7b) – *Observations*: $D_{LR} = 41.3$ km. $d_C \approx 13$ km. $D_2/D_{LR} = 0.98$. Gap around 28 km.

*Model*: $f_{LR} = 0.033$. $D_{PB} \approx 137$ km. Largest remnant shape: Cone-like.

The model does not give a sharp fit to the size distribution of *Koronis*, but it again reproduces its overall characteristics down to the diameter of completeness.

From the model fit it is not straightforward to deduce an estimate for the age of the family.

Two different main estimates of the age of Koronis have been recently given, taking into account the contraints due to the cratering record on *Ida* (Greenberg *et al.* , 1996), and the existence of *Ida–Dactyl* system (Geissler *et al.* , 1996), that belongs to this family. One estimation gives an age $\leq 1.5 Gyr$, and the other one suggests a much younger age, $\approx 50 Myr$.

- *THEMIS* (Fig. 7c) – *Observations*: $D_{LR} = 248.9$ km. $d_C \approx 25$ km. $D_2/D_{LR} = 0.56$.

*Model*: $f_{LR} = 0.2$. $D_{PB} \approx 460$ km. Largest remnant shape: Antipodal sphere.

In this case the model provides quite a good fit to the observed distribution for the 8 largest members, that is down to about 80 km in size. As the completeness size is well below that, it's worth estimating the collisional lifetime of the members of the family, in order to assess if the difference between the model results and the observed size distribution can be attributed to collisional evolution. It is worth noting that the Themis family displays a prominent two-lobed structure, potentially indicative of a prominent secondary collision.

Using a modified version of the collisional evolution code described in Campo Bagatin *et al.* , 1994, it is possible to estimate the rate of depletion of the population of *Themis*. Taking the populations expected if the *Themis* family were originated by an impact for which this model holds, and calculating the depletion rate at different sizes, we see that after about 2.5 Byr we end up close to the populations observed nowadays.

For instance, if we take 2 reference sizes: 50 km and 75 km, we have at present, in the cumulative distribution, 13 and 8 objects respectively. The fragmentation model produces about 35 and 12 objects larger then these sizes. Estimating the depletion rate over the time span mentioned above yields, respectively, 12 to 15 bodies for D$\approx$ 50 km, and 7 to 8 bodies for D$\approx$75 km, and these populations are very close to the actual one, at corresponding sizes.

• *MARIA* (Fig. 7d) – *Observations*: $D_{LR}$ = 48.2 km. $d_C \approx$ 10 km. $D_2/D_{LR}$ = 0.98.

*Model*: $f_{LR}$ = 0.03. $D_{PB} \approx$ 160 km. Largest remnant shape: Antipodal sphere.

This case may be interpreted in a similar way to the *Themis*

family. The model in fact reproduces the overall size distribution down to some 30 km, below this size, erosion of the population due to collisional evolution can be estimated. In order to achieve the nowadays observed populations it is necessary to suppose an age for this family between 3 and 4 Byr.

• *MISA* (Fig. 7e) – *Observations*: $D_{LR}$ = 73 km. $d_C \approx$ 12 km. $D_2/D_{LR}$ = 0.32. Small $D_2/D_{LR}$ and steep distribution for the largest objects.

*Model*: $f_{LR}$ = 0.3. $D_{PB} \approx$ 110 km. Largest remnant shape: Intersection of spheres.

• *ERIGONE* (Fig. 7f) – *Observations*: $D_{LR}$ = 72.6 km. $d_C \approx$ 15 km. $D_2/D_{LR}$ = 0.27. Small $D_2/D_{LR}$ and steep distribution for the largest objects.

*Model*: $f_{LR}$ = 0.3. $D_{PB} \approx$ 108 km. Largest remnant shape: Intersection of spheres.

• *HYGIEA* (Fig. 7g) – *Observations*: $D_{LR}$ = 407.2 km. $d_C \approx$ 25 km. $D_2/D_{LR}$ = 0.22. Small $D_2/D_{LR}$ and steep distribution for the largest objects.

*Model*: $f_{LR}$ = 0.5. $D_{PB} \approx$ 513 km. Largest remnant shape: Antipodal sphere

The fit of the model to the observed populations of these families is very good, especially in the case of Misa. The pattern of the family size distributions is completely reproduced in the case of *Misa* and *Erigone*, respectively for their largest 11 and 5 members, down to about the completeness diameter, around 15 km. It has to be recalled that the former two families are small families (25 members for *Misa*, and 45 members for *Erigone*). For *Hygiea* instead, the agreement is limited to the largest 5 members, and the model size distribution departs from the observed one for the other large–size components of the family, possibly due to collisional evolution. At smaller sizes, observational biases seem to be responsible for the departure from the model predictions.

• *MERXIA* (Fig. 7h) –*Observations*: $D_{LR}$ = 29.6 km. $d_C \approx$ 11 km. $D_2/D_{LR}$ = 0.48.

*Model*: $f_{LR}$ = 0.5. $D_{PB} \approx$ 39 km. Largest remnant shape: Intersection of spheres

Even if this case has to be cautiously considered due to the small size of the members of this family and to the fact that most of the data are below the completeness diameter, again a good agreement is found between the data and the results from the model.

• *GEFION* (Fig. 7i) – *Observations*: $D_{LR}$ = 29.5 km. . $d_C \approx$ 11 km. $D_2/D_{LR}$ = 0.8.

*Model*: $f_{LR}$ = 0.05. $D_{PB} \approx$ 90 km. Largest remnant shape: Intersection of spheres.

In this case the overall behaviour of the size distribution of the fragments produced by the model is in acceptable agreement with observational data, but a greater largest remnant of the impact that formed this family would be required.

• *VESTA* (Fig. 7j) – *Observations*: $D_{LR}$ = 468.3 km. . $d_C \approx$ 10 km. $D_2/D_{LR}$ = 0.02.

*Model*: $f_{LR}$ = 0.9995. $D_{PB}$ = 468.3 km. Largest remnant shape: Intersection of spheres.

In this case the overall behaviour of the size distribution of the fragments produced by the model is in acceptable agreement with observational data. However, given the small size of the secondary fragments, one must remember that they may be collisionally evolved.

Generally speaking, it has to be recalled that any fragmentation model intends to simulate the results of a given impact *at the time it happens*. For an asteroid family, the development of the size distribution subsequent to the generating collision may result in a more or less regular collisional evolution of its members, this evolution may also erode or/and erase some of the largest fragments formerly produced. In this case, when we observe today a family size distribution, we are not observing the original one, but an evolved one, and some of the original largest members may be missing. On the other hand, family data include sometimes some "intruders", the so–called *interlopers*, that is objects that have the same kind of proper elements than the members of the family, but are not "genetically" related to it, they do not come from the impact that generated its proper–element space mates (Migliorini *et al.* , 1995). In these cases we observe and include these bodies in the family data, and this may mislead the interpretation of size distribution.

As a final set of simulations, we also report some of the "bad" results. For *Eunomia* (Fig. 7k), and *Adeona* (Fig. 7l) families we do not manage to fit the observed distribution in such a satisfactory way as we did in other cases, but –as can be seen qualitatively– the average power–law distribution of the intermediate size members of the simulated families are very close to the observed ones.

In all the "good" fits reported here (except for Merxia and Vesta), we find a parent body size wich is larger than the one derived by Tanga *et al.* , by 10 to 20%. This is probably the result of their slight modification of the algorithm, allowing for an overlap of the fragment of up to 20% and fixing the size of the second largest fragment regardless of the geometrical constraints.

# VII Conclusions and Discussion

We have improved Tanga *et al.* model in a way to be able to account for the available volume for the creation of fragments in a more realistic way, as explained in sec. II. A first conclusion that may be argued from what we have shown is that – no matter the shape of the parent body, largest remnant and fragments – if we allow the largest remnant to leave just a shell–like available volume for the production of fragments, we obtain distributions strongly depending on the $f_{LR}$ ratio in the large size range. Allowing for the kind of shapes described in sec. II and III we obtain for the size distribution of fragments – apart the flattening region at smallest sizes – a power–law that has the same exponent for any value of $f_{LR}$. This is an interesting finding at least on a geometric point of view. On the other hand, it is hard to assess that this is also a meaningful finding in the explanation of fragmentation phenomena.

Our further improvements to the fragmentation model – that is the "3–D grid" model (sec. VI) – lead to a set of positive results, that may be summarized in the following items.

i) The model seems to give reasonable and realistic results for the largest members of each family, corresponding to the largest fragments formed as a result of the generating collision. Some characteristic patterns of families distributions may be reproduced. Asteroid families have total numbers of observed members of the order of a few tens or hundreds, and their distributions are irregular at largest sizes; in our model, for the greatest size range, no defined power–law holds either, and we are able to fit many families' distributions fairly well.

ii) Very steep size distributions in the results of the model agree with very steep size distributions of some families ($N(> D) \propto D^{-b}$, with $2.5 \leq b \leq 3.5$).

iii) Various shapes for the largest remnant of any family can be considered, as suggested by experiments, and non-spherical, irregular shapes for any fragment are obtained.

These results have to be handled with care, as it is obvious that some criticism are in order here. In fact, even if this kind of distributions seem to mimic many of the steep observed distributions of asteroid families, it has to be kept in mind that there is *no physics* at all in the model.

The parent bodies which originated the asteroid families were bodies of rather different sizes. As far as we know, both from laboratory experiments and theory, the outcomes of fragmentation events are supposed to be dependent on the size and composition of the impacted body.

Experimental power–laws seem to be sensitive to the target and impact characteristics (Davis & Ryan, 1990; Fujiwara *et al.* , 1977, Capaccioni *et al.* , 1986, Meibom & Balsev, 1996), a pattern we cannot investigate with our model.

An additional caveat is in order here: no reaccumulation of fragments is taken into account in the model either. In the case in which $f_{LR}$ is supposed to be large, this could mean that that largest member is a reaccumulated object, rather than a monolithic fragment, and we would fail in modelling correctly the originating event. In the case of small $f_{LR}$ we instead can expect that the event generating the family had been extremely energetic, leading to fragmentation and subsequent dispersion of fragments, with no substantial reaccumulation. In these case the present model instead could be useful in reproducing the collisional event that gave birth to the family.

In any case, we think that this work, together with the former one by Tanga *et al.* , point out that the role of geometric constraints in fragmentation phenomena cannot be ruled out from comprehensive models of fragmentation. And even if this role has to be clarified by further investigations, the present model may be handled as a useful heuristic method to try and fit many steep asteroid families distributions.

# Acknowledgements

A. Campo Bagatin worked on this project in 1998–1999 while staying at the Observatoire de la Côte d'Azur in Nice, thanks to the "Henry Poincaré" fellowship of the Centre National de la Recherche Scientifique.

# References

Campo Bagatin, A., Cellino, A., Davis, D.R., Farinella, P. and Paolicchi, P. 1994. Wavy size distributions for collisional systems with a small-size cutoff. *Planet. Space Sci.* **42,** 1079–1092.

Capaccioni, F., Cerroni, P., Coradini, M., Di Martino, M., Farinella, P., Flamini, E., Martelli, G., Paolicchi, P., Smith, P.N., Woodward, A. and Zappalà, V. 1986. Asteroidal catastrophic collisions simulated by hypervelocity impact experiments. *Icarus* **66,** 487–514.

Davis, D.R. and Ryan, E. 1990. On collisional disruption - Experimental results and scaling laws. *Icarus* **83,** 156–182.

Dohnanyi, J.S. 1969. Collisional Model of Asteroids and Their Debris. *J. geophys. Res.* **74,** 2531–2554.

Farinella, P., Davis, D.R. and Marzari, F. 1996. Asteroid Families, Old and Young. *Completing the Inventory od the Solar System (T.W.Retting and J.M.Hahn eds.), ASP Conf Series* **107,** 45–55.

Fujiwara, A., Kanimoto, G. and Tsukamoto, A. 1977. Destruction of Basaltic Bodies by High-velocity Impacts. *Icarus* **31,** 277–288.

Geissler, P., Petit, J-M., Durda, D., Greenberg, R., Bottke, W., Nolan, M. and Moore, J. 1996. Erosion and Ejecta Reaccretion on 243 Ida and Its Moon. *Icarus* **120,** 140–157.

GILVARRY, J.J. 1961. Fracture of Brittle Solids, I, Distribution Function for Fragment Size in Single Fracture (Theoretical). *J. Appl. Phys.* **32,** 391–399.

GRADIE, J.C. 1978. An astrophysical study of the minor planets in the Eos and Koronis asteroid families. *Ph.D. disseration*, University of Arizona.

GRADY, D.E. AND KIPP, M.E. 1985. Geometric Statistics and Dynamic Fragmentation. *J. Appl. Phys.* **58,** 1210–1222.

GREENBERG, R., BOTTKE, W., NOLAN, M., GEISSLER, P., PETIT, J-M., DURDA D., ASPHAUG, E. AND HEAD, J. 1996. Collisional and Dynamical History of Ida. *Icarus* **120,** 106–118.

HIRAYAMA K. 1933. Present State of the Families of Asteroids. *Proc. Imp. Acad., Tokyo* **9,** 482–485.

LIENAU, C.C. 1936. Random Fracture of brittle Solids. *J.Franklin Inst.* **221,** 485–494, 674–686, 769–783.

MEIBOM, A. AND I. BALSEV 1996. Composite power laws in shock fragmentation. *Ph. Rev. Lett.* **76,** 2492–2494.

MIGLIORINI, F., ZAPPALA, V., VIO, R. AND CELLINO, A. Interlopers within asteroid families. *Icarus* **118,** 271–291.

MOTT, N.F. 1947. Fragmentation of Shell Cases. *Proc. R. Soc. Lon.* **300,** 300–308.

PAOLICCHI, P., VERLICCHI, A. AND CELLINO, A. 1996. An Improved Semi-Empirical Model of Catastrophic Impact Processes. I: Theory and Laboratory Experiments. *Icarus* **121,** 126–157.

PETIT, J-M. AND FARINELLA, P. 1993. Modelling the outcomes of high-velocity impacts between small solar system bodies. *Celest. Mech.* **57,** 1–28.

ROSIN,P. AND RAMMLER, E. 1933. The Laws Governing the Fineness of Powdered Coal. *Inst.Fuel* **7,** 29–36.

TANGA, P., CELLINO, A., MICHEL, P., ZAPPALÁ, V., PAOLICCHI, P.AND DELL'ORO, A. 1999. On the Size Distribution of Asteroid Families: the Role of Geometry. *Icarus* **141,** 65–78.

ZAPPALÁ, V. AND CELLINO, A. 1996. Main Belt Asteroids: Present and Future Inventory. *Completing the Inventory od the Solar System (T.W.Retting and J.M.Hahn eds.), ASP Conf Series* **107,** 29–44.

# Figure captions

Figure 1: Section of the spheres defining the largest fragment by a plane containing the $x$-axis. The solid line contours the largest remnant while the dashed lines represent the rest of the spheres. (a): $f_{LR} \geq 27/32$. (b): $27/32 \geq f_{LR} \geq 1/8$. (c) $1/8 \geq f_{LR}$

Figure 2: Cumulative size distribution of fragments for each value of $f_{LR}$ in 0.1, 0.3, 0.5, 0.7, 0.9.

Figure 3: Ratio of the size of the second largest fragment to the size of the parent body as a function of $f_{LR}$. Open circles: this model; solid circles: Tanga *et al.* model.

Figure 4: Ratio of the total volume of the fragments to the volume of the parent body volume, as a function of $f_{LR}$. Open circles: this model; solid circles: Tanga *et al.* model.

Figure 5: Mean power–law exponent in the range [300, 3000] fragments, as a function of $f_{LR}$, averaged over 20 simulations.

Figure 6: A representation of a section of the 3D–grid model, illustrating the fragments production.

Figure 7: Fits of the model to asteroid families. The dashed lines give the completeness diameter, when known.

| $f_{LR}$ | spheres | cubes | parallelepipeds |
|---|---|---|---|
| 0.1 | 0.60 | 0.70 | 0.92 |
| 0.3 | 0.68 | 0.74 | 0.93 |
| 0.5 | 0.77 | 0.84 | 0.94 |
| 0.7 | 0.87 | 0.86 | 0.95 |
| 0.9 | 0.95 | 0.94 | 0.97 |

Table 1: The ratio of recovered volume over the parent body volume is given, as a function of $f_{LR}$ and of the model adopted for the shape of the parent body and the fragments.

| Asteroid Family | $D_{LR}$ | $d_C$ | $D_2/D_{LR}$ | $f_{LR}$ | $D_{PB}$ | shape |
|---|---|---|---|---|---|---|
| EOS | 103.9 | 17 | 0.84 | 0.1 | 240 | A.S. |
| KORONIS | 41.3 | 13 | 0.98 | 0.033 | 137 | S.C. |
| THEMIS | 248.9 | 25 | 0.56 | 0.2 | 460 | A.S. |
| MARIA | 48.2 | 10 | 0.98 | 0.03 | 160 | A.S. |
| MISA | 73 | 12 | 0.32 | 0.3 | 110 | I.S. |
| ERIGONE | 72.6 | 15 | 0.27 | 0.3 | 110 | I.S. |
| HYGIEA | 407.2 | 25 | 0.22 | 0.5 | 513 | A.S. |
| MERXIA | 29.6 | 11 | 0.48 | 0.5 | 39 | I.S. |
| GEFION | 29.5 | 11 | 0.8 | 0.05 | 90 | I.S. |
| VESTA | 468.5 | 10 | 0.02 | 0.9995 | 468.3 | I.S. |

Table 2: For any given family observational data are reported in the first three columns: the size of the largest observed member ($D_{LR}$), the completeness diameter ($d_C$), and the ratio between the two largest members ($D_2/D_{LR}$); the corresponding results of the model are summarized in columns 4, 5 and 6: 'Largest Fragment Mass/Parent Body Mass' ($f_{LR}$), parent body size ($D_{PB}$), and largest remnant shape. All sizes are given in km. A.S.: Antipodal Sphere. I.S.: Intersection of Spheres. S.C.: Straight Cone.

Figure 1; Campo Bagatin, A. and Petit, J-M.

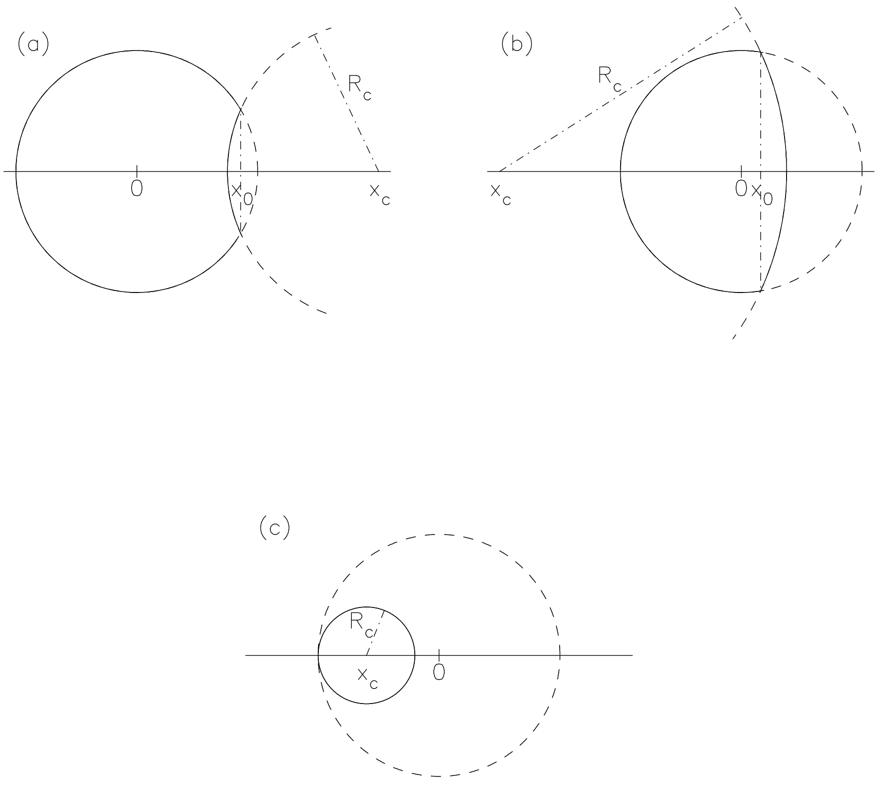

Figure 2; Campo Bagatin, A. and Petit, J-M.

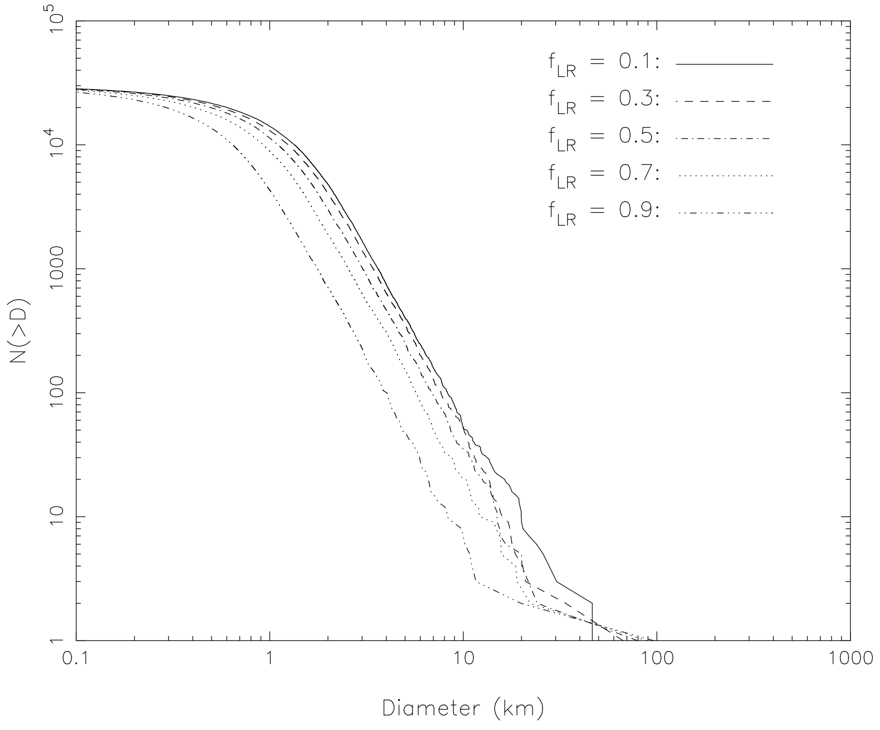

Figure 3; Campo Bagatin, A. and Petit, J-M.

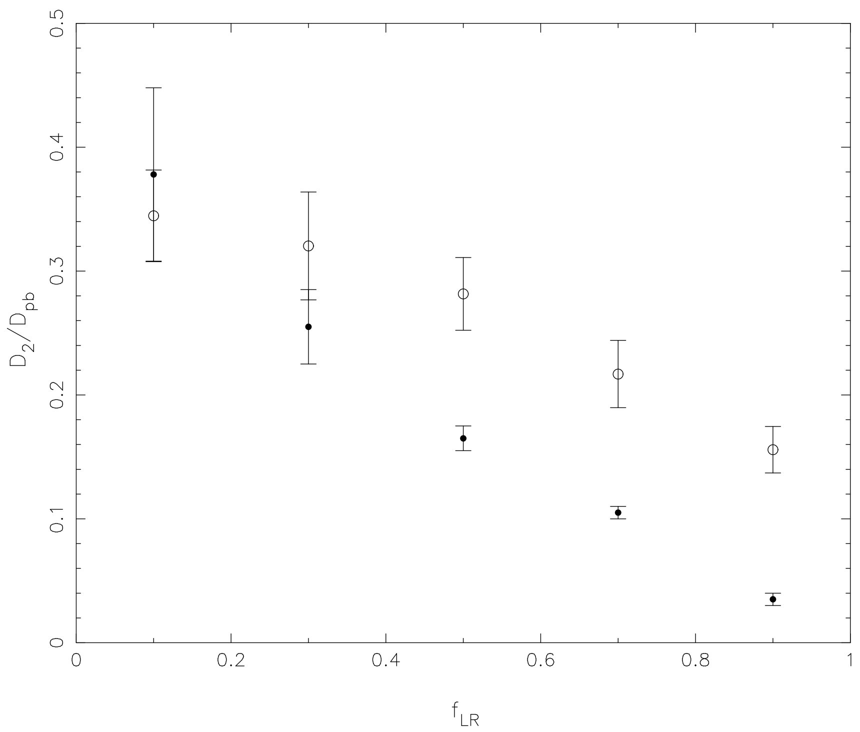

Figure 4; Campo Bagatin, A. and Petit, J-M.

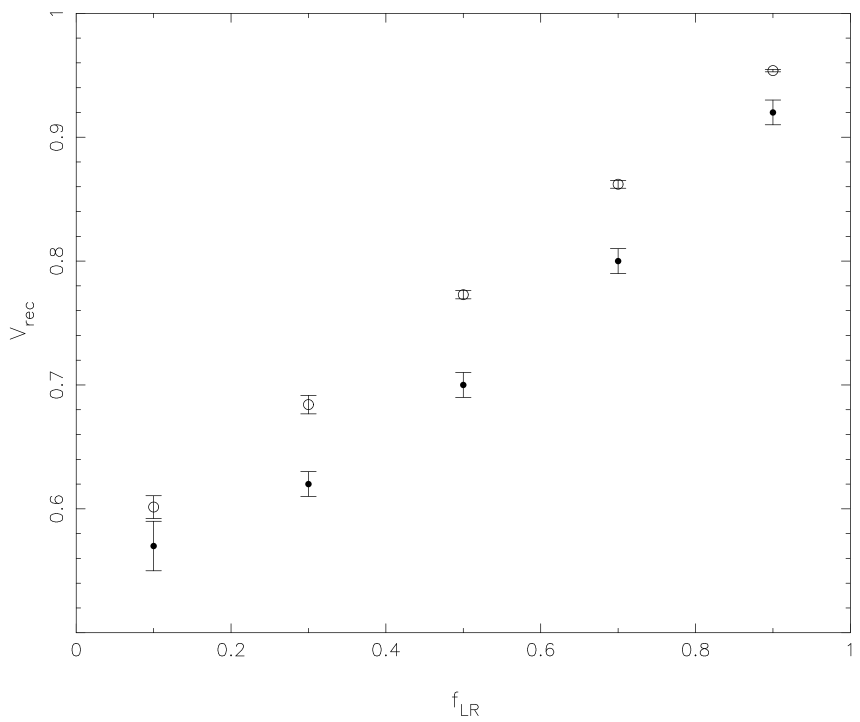

Figure 5; Campo Bagatin, A. and Petit, J-M.

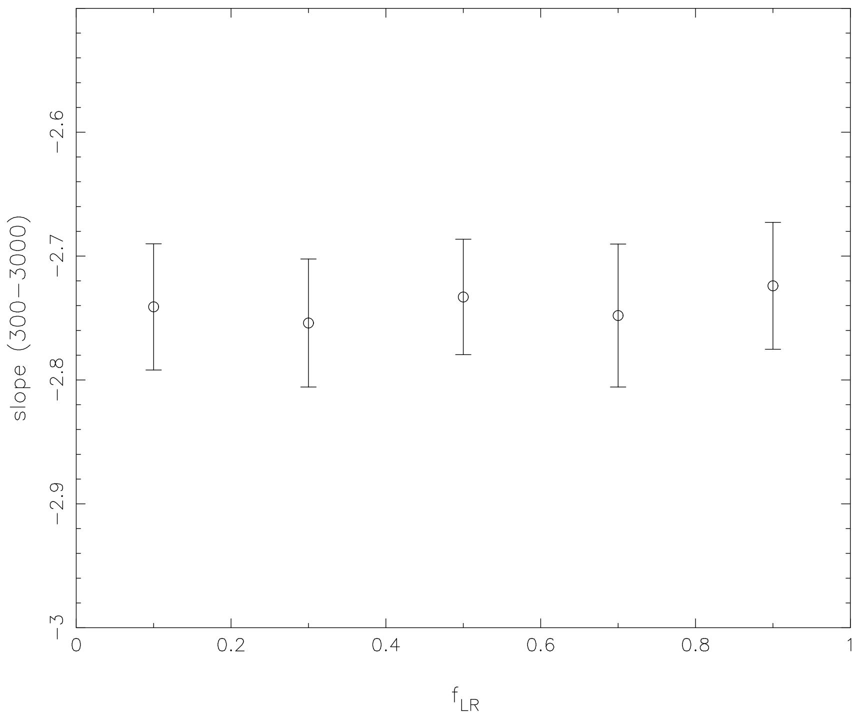

Figure 6; Campo Bagatin, A. and Petit, J-M.

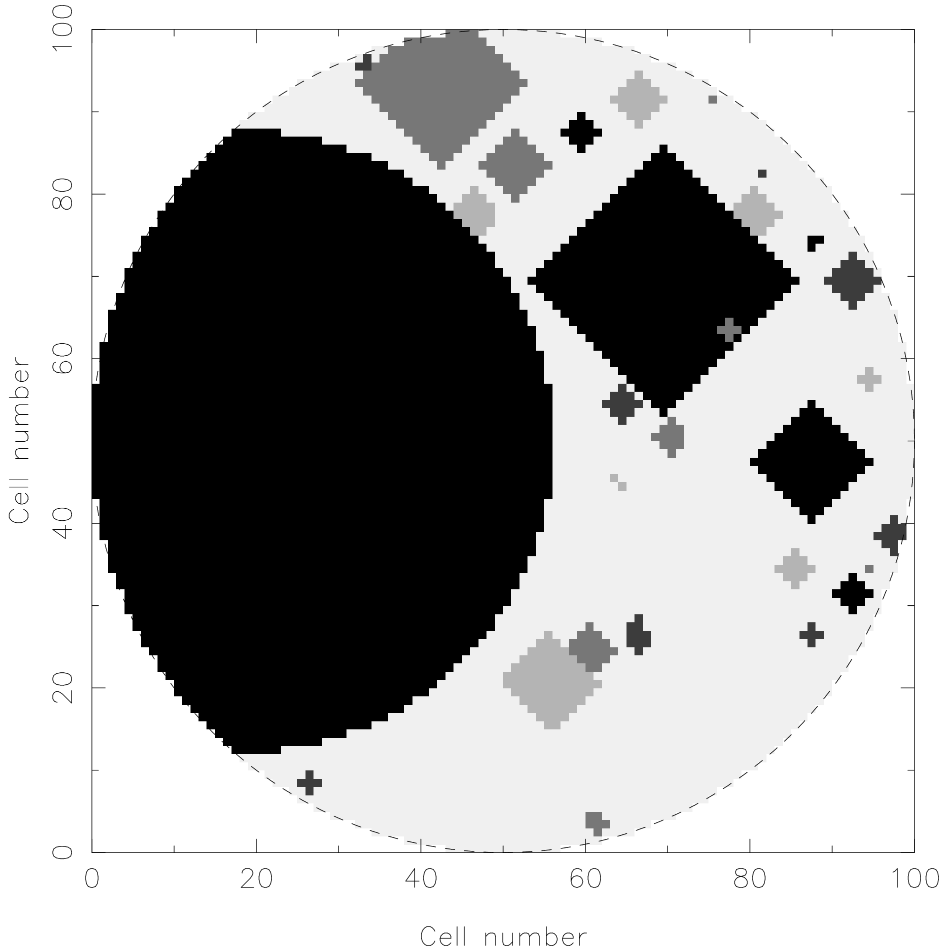

Figure 7; Campo Bagatin, A. and Petit, J-M.

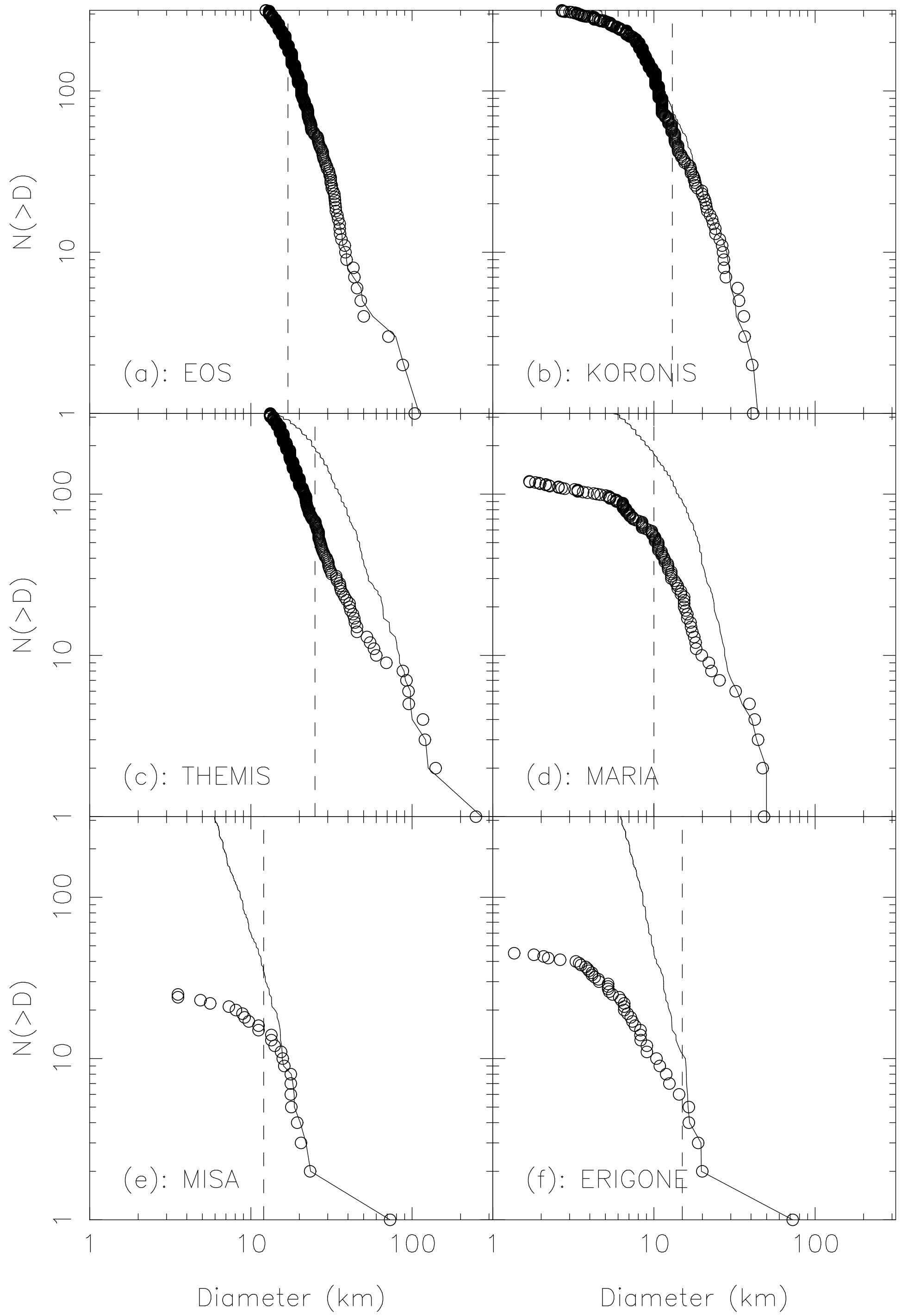

Figure 7 continued; Campo Bagatin, A. and Petit, J-M.